DEVELOPMENTS IN A LOW-REYNOLDS NUMBER NONLINEAR EDDY-VISCOSITY MODEL FOR FLOWS WITH COMPLEX STRAINS

Tim J. Craft
School of Mechanical, Aerospace and Civil Engineering,
The University of Manchester,
P.O. Box 88, Manchester M60 1QD, UK
Tim.Craft@manchester.ac.uk

Michael T. Deevy*
School of Mechanical, Aerospace and Civil Engineering,
The University of Manchester,
P.O. Box 88, Manchester M60 1QD, UK

ABSTRACT

Non-linear eddy-viscosity schemes can potentially return better predictions than linear schemes in flows with complex strains, including flow separation and impingement and three-dimensional boundary layers. In their study of separated flow over a 2D hill, Abe et al. (2002) tested numerous models, and identified the non-linear EVM of Abe et al. (2003) as performing the best. The model was proposed in two forms: one based on solving an ε equation (denoted AJL-ε), and one in which an ω equation provided the lengthscale (AJL-ω). The present work has further tested the model forms proposed by Abe et al. (2003) in a range of challenging flows. The ε-based scheme is found to perform more reliably, and a number of modifications have been proposed to broaden its width of applicability.

INTRODUCTION

It is well known that linear eddy-viscosity models do not reproduce many of the features found in flows with complex strain fields. Stress transport schemes have the potential to perform much better, but at a greater computational cost. For this reason there has been significant interest in the use of non-linear eddy-viscosity schemes that can be applied to flows with complex strains, including flow separation and impingement and three-dimensional boundary layers.

In their study of separated flow over a 2D hill, Abe et al. (2002) tested numerous models, and identified the non-linear EVM of Abe et al. (2003) as performing the best. In the present work modelling refinements to the AJL-ε are proposed. First, the original AJL model is briefly described then the present modifications are detailed. Results with the modified AJL-ε model and the two original variants of the AJL model are shown for two different skewed flows, accelerating boundary layers, and impinging flows.

THE ABE ET AL. (2003) MODEL

This model is based on an exact inversion of an algebraic stress model (ASM) in two-dimensions. Hence, the constitutive equation is reduced to the following

$$\begin{aligned} a_{ij} &= \beta_1\tau S_{ij} + \beta_2\tau^2(\Omega_{ik}S_{kj} - S_{ik}\Omega_{kj}) \\ &\quad +\beta_3\tau^2(S_{ik}S_{kj} - \frac{1}{3}S_{kl}S_{kl}\delta_{ij}) \end{aligned} \quad (1)$$

Although the model is based on an inversion of an ASM, only the form of the resulting nonlinear tensorial expression and the relative sizes of the terms are used: the functions employed for the coefficients have been tuned by reference to a number of theoretical and practical flow configurations. The turbulent timescale, rate of strain and rotation tensors in equation (1) are

$$\tau = \frac{k}{\varepsilon} \quad S_{ij} = \frac{\partial U_i}{\partial x_j} + \frac{\partial U_j}{\partial x_i} \quad \Omega_{ij} = \frac{\partial U_i}{\partial x_j} - \frac{\partial U_j}{\partial x_i} \quad (2)$$

The coefficient of the tensorially linear term is

$$\beta_1 = -C_B(c_\mu f_\mu + f_{s1}c_\mu^2 f_\mu^2 \tau^2 C_D^2(\Omega^2 - S^2)) \quad (3)$$

where

$$C_B = \frac{1}{1 + \frac{22}{3}c_\mu^2 f_\mu^2 C_D^2 \frac{\tau^2}{2}\Omega^2 + \frac{2}{3}c_\mu^2 f_\mu^2 C_D^2 \frac{\tau^2}{2}(\Omega^2 - S^2)f_B} \quad (4)$$

and $c_\mu = 0.12$, $C_D = 0.8$

$$f_\mu = (1 + 35(Re_t/30)^{-3/4}\exp[-(Re_t/30)^{3/4}]f_w(26) \quad (5)$$

$$f_B = 1 + 100c_\mu f_\mu \frac{\tau}{\sqrt{2}}(\Omega - S) \quad (6)$$

and

$$f_{s1} = -f_{r1}f_{r2}C_{s1}c_\mu^2 f_\mu^2 \frac{\tau^2}{2}(\Omega^2 - S^2) \quad (7)$$

where $S = \sqrt{S_{ij}S_{ij}/2}$ and $\Omega = \sqrt{\Omega_{ij}\Omega_{ij}/2}$. The near-wall damping term f_μ uses the following function:

$$f_w(A) = \exp[-(n^*/A)^2] \quad (8)$$

where n^* is the non-dimensional wall distance defined as $n^* = u_\varepsilon n/\nu$ (n is the wall normal distance and u_ε is the Kolmogorov velocity scale). Abe et al. (1997) found this form of near-wall damping brought about significant improvements in separated flows. The quadratic terms are as follows:

$$\beta_2 = (1 - f_w(26))\beta_2^{(1)} + f_w(26)\beta_2^{(2)} \quad (9)$$

*Corresponding author, now with the Health and Safety Laboratory, Harpur Hill, Buxton, Derbyshire SK17 9JN, UK Mike.Deevy@hsl.gov.uk

$$\beta_3 = (1 - f_w(26))\beta_3^{(1)} + f_w(26)\beta_3^{(2)} \quad (10)$$

where

$$\beta_2^{(1)} = C_B c_\mu^2 f_\mu^2 C_D/2 \quad (11)$$

$$\beta_3^{(1)} = C_B c_\mu^2 f_\mu^2 C_D(1 + f_{s2})/2 \quad (12)$$

and $f_{s2} = -f_{r1}f_{r2}\{1 + C_{s2}c_\mu f_\mu \frac{\tau}{\sqrt{2}}(\Omega - S)\}$. The constants c_μ and C_D are tuned to represent correctly equilibrium wall turbulence and homogeneous shear flow. The response of the anisotropy components has been tested in a number of fundamental flows (Abe et al., 2003), showing that realizability is maintained. However, the quadratic terms become zero as the wall is approached, where the EASM assumptions become untenable. The following terms are included to account for near-wall anisotropy:

$$\beta_2^{(2)} = 0.5(1 - f_{r1}^2)\frac{\beta_w C_w C_D^2}{1 + 0.5C_w C_D^2 \tau_d^2 \sqrt{S^2\Omega^2}} \quad (13)$$

$$\beta_3^{(2)} = -0.5(1 - f_{r1}^2)\frac{\gamma_w C_w C_D^2}{1 + 0.5C_w C_D^2 \tau_d^2 S^2} \quad (14)$$

and $\beta_w = \frac{1}{4}, \quad \gamma_w = 1.5, \quad C_w = 0.5$. The near-wall timescale is defined as $\tau_d = \{1 - f_w(15)\}\frac{k}{\varepsilon} + f_w(15)\{\frac{\sqrt{\nu}}{\varepsilon}\}$. There is also the following additional near-wall term in the constitutive equation:

$$a'_{ij} = a_{ij} - C_D f_w(26)\frac{1}{2}(d_i d_j - d_k d_k \delta_{ij}/3) \quad (15)$$

where a_{ij} is the anisotropy tensor defined in equation (1) and

$$d_i = \frac{N_i}{\sqrt{N_k N_k}} \qquad N_i = \frac{\partial l_d}{\partial x_i} \qquad l_d = n \quad (16)$$

In contrast to most eddy-viscosity models, the AJL model does not use a single eddy-viscosity in both the constitutive equation and the turbulence transport equations. Instead, the eddy-viscosity employed in the diffusion terms of the latter is defined as

$$\nu_t = c_\mu f_\mu \frac{k^2}{\varepsilon} \quad (17)$$

which does not include damping due to strain rate and vorticity. The k-equation can be written as follows:

$$\frac{Dk}{Dt} = \frac{\partial}{\partial x_j}\left\{\left(\nu + \frac{\nu_t}{\sigma_k}\right)\frac{\partial k}{\partial x_j}\right\} + P_k - \varepsilon \quad (18)$$

Versions of the AJL model have been developed with two different lengthscale determining equations (ε and ω). Both models use the same constitutive equation and k-equation, as described above, which therefore enables one to investigate the relative strengths and weaknesses of the ε and ω-equations with fewer unrelated differences between models that tend to confuse matters. The ε-equation can be written as follows:

$$\frac{D\varepsilon}{Dt} = \frac{\partial}{\partial x_j}\left\{\left(\nu + \frac{\nu_t}{\sigma_\varepsilon}\right)\frac{\partial \varepsilon}{\partial x_j}\right\} + C_{\varepsilon 1} f_1 \frac{\varepsilon}{k} P_k - C_{\varepsilon 2} f_2 \frac{\varepsilon^2}{k} \quad (19)$$

The ω-equation is based on a transformation of the above ε-equation:

$$\frac{D\omega}{Dt} = \frac{\partial}{\partial x_j}\left\{\left(\nu + \frac{\nu_t}{\sigma_\omega}\right)\frac{\partial \omega}{\partial x_j}\right\} + \alpha\frac{\omega}{k}P_k - \beta\omega^2 + E_\omega \quad (20)$$

The high-Reynolds-number forms of the coefficients are retained from the ε-equation, although the near-wall damping terms are slightly different. A cross diffusion term is retained from the transformation (together with a function that ensures it is only active away from a wall) to remove the freestream sensitivity problem often associated with ω equations.

MODELLING REFINEMENTS

After examining a number of test cases, two key features have been incorporated into the AJL-ε model. Firstly, the following near-wall gradient production term has been included in the ε equation, in order to give the desired sensitivity in flows with strongly varying near-wall strains:

$$P_{\varepsilon 3} = \big(C_{\varepsilon 3}\nu\frac{k}{\varepsilon}\overline{u_i u_j}\frac{\partial^2 U_k}{\partial x_i \partial x_l}\frac{\partial^2 U_k}{\partial x_j \partial x_l} + \frac{C_{\varepsilon 4}}{2}\nu\frac{k}{\varepsilon}\frac{\partial \overline{u_i u_j}}{\partial x_i}\frac{\partial U_l}{\partial x_k}\frac{\partial^2 U_l}{\partial x_k \partial x_j}\big)\exp\left\{-\left(\frac{Re_t}{250}\right)^3\right\} \quad (21)$$

where

$$C_{\varepsilon 3} = 0.72 \;\; C_{\varepsilon 4} = 0.9 \quad (22)$$

Secondly, the following differential lengthscale correction is introduced to the ε equation:

$$S_\varepsilon = 0.1\sqrt{S_I{}^2}\,\min(0.1, \widetilde{Re_t}/5.0)\frac{\tilde{\varepsilon}^2}{k}\max(F(F+1)^2, 0.0) \quad (23)$$

where

$$F = [(\partial l/\partial x_j)(\partial l/\partial x_j)^{1/2} - dl_e dy]/c_l \quad (24)$$

$$l = k^{3/2}/\varepsilon \quad (25)$$

$$dl_e dy = c_l[1 - \exp(-B_\varepsilon \widetilde{Re_t})] + B_\varepsilon c_l \widetilde{Re_t}\exp(-B_\varepsilon \widetilde{Re_t}) \quad (26)$$

and

$$c_l = 2.55, B_\varepsilon = 0.1069, S_I = S_{ij}S_{jk}S_{ki}/(S_{nl}S_{nl}/2)^{3/2} \quad (27)$$

The above is a modified form of the lengthscale correction proposed by Raisee (1999), and is included to particularly aid the prediction of stagnating flow regions. Further improvements in stagnating flows were obtained by introducing an additional contribution to C_B, designed to reduce this coefficient in regions of strong normal straining:

$$C_B = \frac{1}{1 + \frac{22}{3}c_\mu^2 f_\mu^2 C_D^2 \frac{\tau^2}{2}\Omega^2 + \frac{2}{3}c_\mu^2 f_\mu^2 C_D^2 \frac{\tau^2}{2}(\Omega^2 - S^2)f_B + SS} \quad (28)$$

where

$$SS = 0.141\max(k/\varepsilon\sqrt{(\tau S - 3.333)}, 0.0))\sqrt{(S_I{}^2)} \quad (29)$$

Finally, the terms γ_w and β_w in the constitutive equation were modified as follows:

$$\gamma_w = 1.5(0.7 + 0.3 f_w(15)) \;\; , \;\; \beta_w = 0.25(0.7 + 0.3 f_w(15)) \quad (30)$$

in order to improve numerical stability in near-wall regions with strong and rapidly-varying strain rates.

COMPUTATIONAL RESULTS

The resulting scheme has been tested in plane channel and equilibrium boundary layer flows. For these flows there is a negligible difference between the results with the original AJL-ε model and this new version. Jang (2004) has reported that the modified scheme performs equally as well as the original AJL-ε model did in the separated flow over a 2D hill. Below,

the modified AJL-ε model is tested in flows involving skewness, acceleration and impingement.

SKEWED SHEAR FLOWS

The DNS of Howard and Sandham (2000) is a fully developed channel flow ($Re_\tau = 180$) in which both walls are given a sudden velocity perpendicular to the flow direction, creating a shear-driven three-dimensional wall layer. The challenging feature of the flow development is that the DNS data show an initial decrease of the peak shear stress and turbulence energy levels. There is a subsequent recovery in both quantities as the flow realigns and returns towards a fully developed state. Figure 1 shows the shear stress $-\overline{uv}^+$ profile at non-dimensional times $t = 0.0$, 0.3, 0.4 and 1.0. For early times ($t < 0.3$) the shear stress reduces by up to 40% around $y^+ = 30$. It then begins to increase near the wall as the flow realigns (from $t = 0.4$), until by $t = 1.0$ it has returned to levels similar to those of the original 2D channel flow.

Neither of the original AJL forms capture any of the shear stress response shown in the data, whereas the modified form does, at least to a certain extent, predict the decrease and subsequent growth of $-\overline{uv}^+$. One finding of the study was that it was only models that did include a near-wall gradient-production type of term in the lengthscale-governing equation which could return even qualitatively correct results in this case.

Kannepalli and Piomelli (2000) carried out an LES of a related flow. This was a zero pressure gradient boundary layer (at $Re_\theta = 1,100$) in which a section of the wall moved in the spanwise direction with velocity equal to that of the freestream. Figure 2 shows the mean velocity profiles at a number of streamwise locations on and after the moving section of wall (normalized with a reference displacement thickness, δ_r^*, corresponding to 1% of the moving wall length). In this case one can see a clear velocity 'deficit' region caused by changes to the shear stress. Results with the three versions of the AJL model again show that only the modified AJL-ε scheme predicts profiles that are broadly in line with those of the LES data. Figure 3 show the shear stress $\overline{uv}/U_\infty$ for the three versions of the AJL model. Only the modified AJL-ε model broadly captures the changes in shear stress seen in the LES.

Figure 4 shows the skin friction in the streamwise direction for the case with zero spanwise shear ($W_r = 0.0$). Figure 5 shows c_{f_x} for the case with spanwise velocity equal to that of the freestream ($W_r = 1.0$). The qualitative changes in spanwise skin friction seen in the LES data are reproduced at least to some extent by the modified AJL-ε model. The other two versions of the model show an incorrect response to the spanwise shear. Figure 6 shows the spanwise skin friction, whose magnitude sharply increases as the shear is introduced. The modified AJL-ε model returns the results closest to the LES, although the magnitude is still overpredicted.

SINK FLOW BOUNDARY LAYERS

The direct simulations of Spalart (1986) provide a simple test case in which the performance of turbulence models under strong acceleration can be assessed. Sink flows can be characterised by the acceleration parameter K, defined by

$$K \equiv \nu/U_\infty^2 \left(\frac{dU_\infty}{dx}\right), \tag{31}$$

where ν is the kinematic viscosity and x the streamwise coordinate.

Figure 7 shows the mean velocity profiles for four different acceleration parameters, ranging from zero up to a very strongly accelerated case with $K = 2.75 \times 10^{-6}$. The DNS data show that the mean velocity profile tends to 'lift' above the line of the log-law as K is increased. Both versions of the model using an ε-equation return broadly the correct response to acceleration. In contrast, the AJL-ω model shows the opposite trend to the DNS data, with the mean velocity profile lying *below* the log-law line at the higher acceleration parameters. This failure to predict the changes in mean velocity is caused by overprediction of the turbulent shear stress and skin friction coefficient. Figure 8 shows shear stress for two different acceleration parameters. The modified AJL-ε model returns the correct profile at both acceleration parameters. In contrast, the AJL-ω overpredicts the shear stress.

IMPINGING FLOWS

The axisymmetric impinging jet involves a number of different flow phenomena, and as such provides a useful test case for the assessment of the proposed model. Figure 9 shows the predicted Nusselt number from a jet impinging on to a flat plate from a height of 2 jet diameters at Reynolds numbers of 23,000 and 70,000 (experiments of Baughn et al., 1992). The original AJL-ε scheme returns reasonable results for the lower Reynolds number case, but predicts too high levels of Nusselt number for the $Re = 70,000$ case, as a result of predicting near-wall turbulence levels which increase too rapidly as the wall jet develops. The modified AJL-ε model performs much better, and successfully captures the shape of the Nusselt number profile at both Reynolds numbers (although the magnitude is slightly overpredicted at the higher Reynolds number). The improvements are mainly due to the inclusion of the lengthscale correction in the ε equation and the modification to the constitutive equation designed to reduce the turbulent viscosity in regions of strong normal straining. Figures 10 and 11 show Nusselt number profiles for discharge heights of 4 and 6 jet diameters. The modified AJL-ε model captures the changes in profile shape for the different heights quite well, although the shape of the profile for $Re = 70,000$, $H/D = 6.0$ is not in such good agreement with the experimental data as other cases.

Figure 12 shows corresponding mean velocity profiles for the impinging jet at at $H/D = 6$ and $Re = 70,000$. Profiles are shown at radial distances of 0, 0.5 and 2.5 diameters from the jet centreline, and the modified AJL-ε scheme is seen to capture the peak velocity more reliably than the other models tested.

CONCLUSIONS

Abe et al. (2002) identified the AJL nonlinear EVM's as producing the most promising results in flows over curved surfaces. Refinements have been made to the ε-based variant of this scheme in order to improve its performance in flows exhibiting strong near-wall skewing and impingement. The resulting model has been shown to return significantly improved results in a number of flows.

ACKNOWLEDGEMENTS

M. T. Deevy acknowledges with thanks the support of BAE

systems and EPSRC for funding this research.

REFERENCES

Abe, K. and Jang, Y.-J. and Leschziner, M.A., 2002, "Investigation of anisotropy-resolving turbulence models by reference to highly-resolved LES data for separated flow", *Flow, Turbul. Combust.*, Vol. 69, pp. 161-204.

Abe, K. and Jang, Y.-J. and Leschziner, M.A., 2003, "Investigation of wall-anisotropy expressions and length-scale equations for non-linear eddy-viscosity models", *Internat. J. Heat Fluid Flow*, Vol. 19, pp. 181-198.

Abe, K. and Kondoh, T. and Nagano, Y., 1997, "On Reynolds-stress expressions and near-wall scaling parameters for predicting wall and homogeneous turbulent shear flows", *Internat. J. Heat Fluid Flow*, Vol. 18, pp. 266-282.

Baughn, J. W., Yan, X. and Mesbah, M., 1992, "The effect of Reynolds number on the heat transfer distribution from a flat plate to a turbulent impinging jet, *ASME winter Annual Meeting*

Cooper, D., Jackson, D. C., Launder, B. E. and Liao, G. X., 1993, "Impinging jet studies for turbulence model assessment – I. Flow-field experiments", *Internat. J. Heat Mass Transfer*, Vol. 36, pp. 2675-2684.

Howard, R. A. and Sandham, N. D, 2004, "Simulation and Modelling of a Turbulent Skewed Channel Flow", *Flow, Turbul. Combust.*, Vol. 65, pp. 83-109.

Jang, Y.-J., 2004, Private communication.

Kannepalli, C. and Piomelli, U., 2000, "Large-eddy simulation of a three-dimensional shear-driven turbulent boundary layer", *J. Fluid Mech.*, Vol. 423, pp. 175-203.

Raisee, M., 1999, "Computation of flow and heat transfer through two- and three-dimensional rib-roughened passages", Ph.D. Thesis, University of Manchester Institute of Science and Technology.

Spalart, P. R., 1986, "Numerical study of sink-flow boundary layers", *J. Fluid Mech.*, Vol. 172, pp. 307-328.

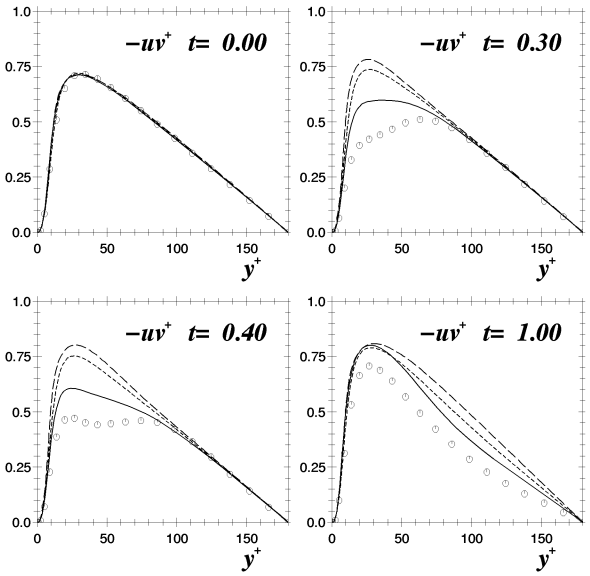

Figure 1: Streamwise shear stress in skewed channel flow

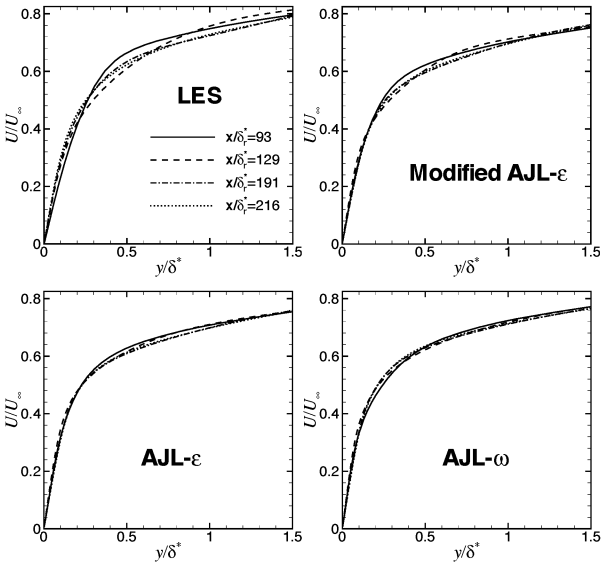

Figure 2: Streamwise mean velocity in the 3D skewed boundary layer flow of Kannepalli and Piomelli (2000)

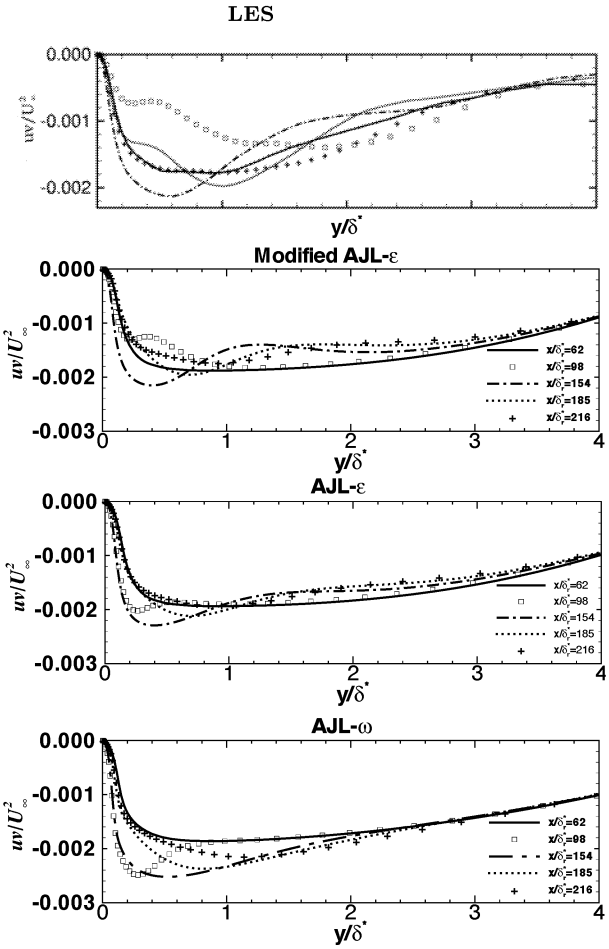

Figure 3: Streamwise shear stress in the 3D skewed boundary layer flow of Kannepalli and Piomelli (2000)

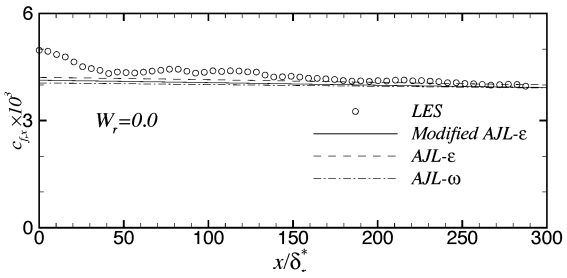

Figure 4: Streamwise variation of the skin friction coefficients in the 3D skewed boundary layer flow of Kannepalli and Piomelli (2000)

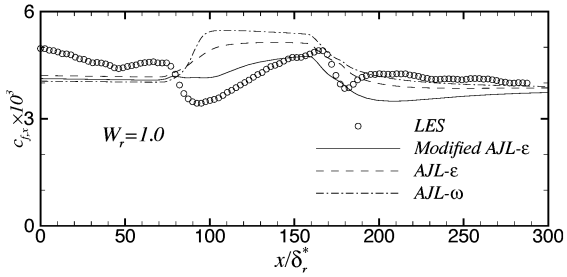

Figure 5: Streamwise variation of the skin friction coefficients in the 3D skewed boundary layer flow of Kannepalli and Piomelli (2000)

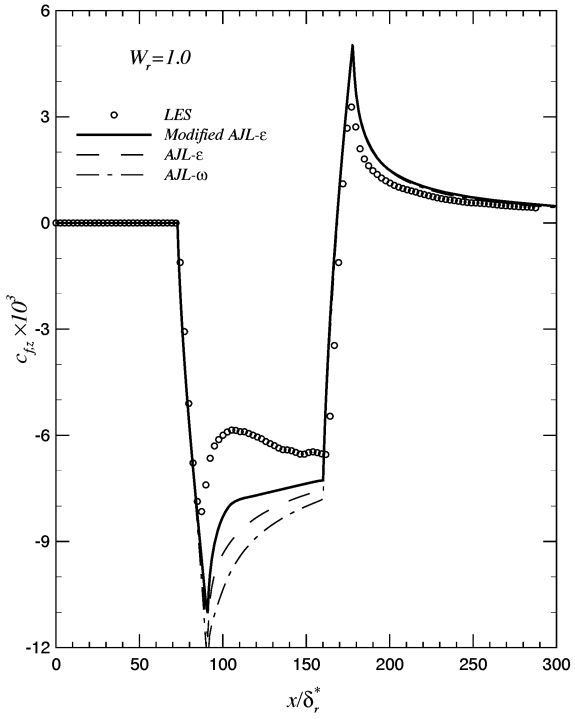

Figure 6: Streamwise variation of the spanwise skin friction coefficient in the 3D skewed boundary layer flow of Kannepalli and Piomelli (2000)

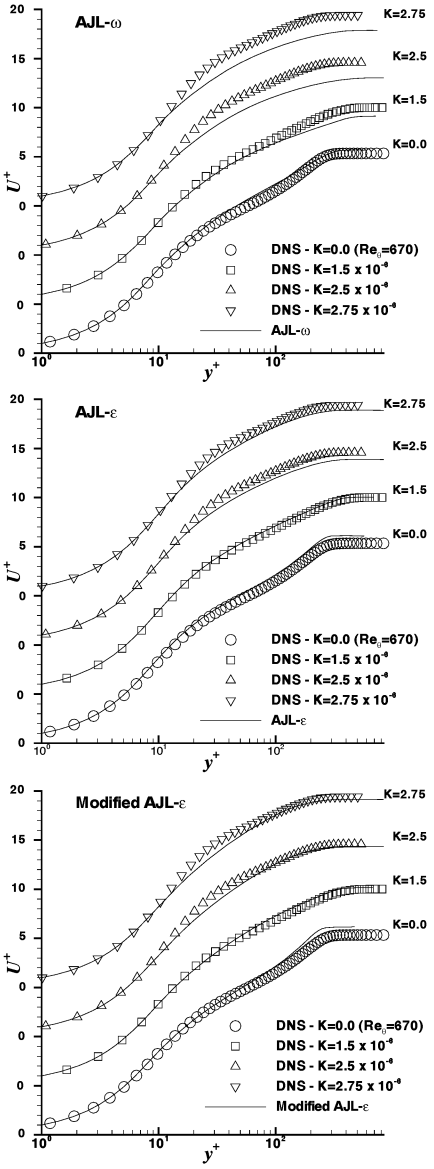

Figure 7: Mean velocity profiles in sink flows

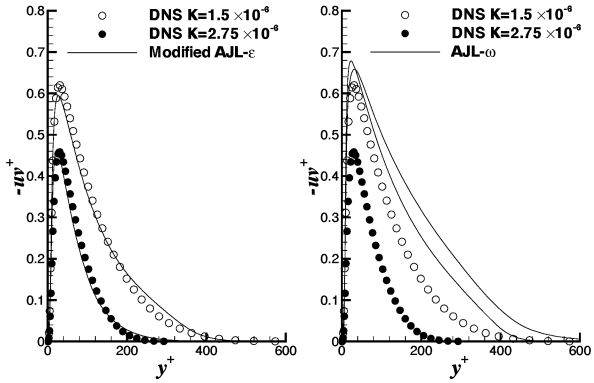

Figure 8: Shear stress in sink flows

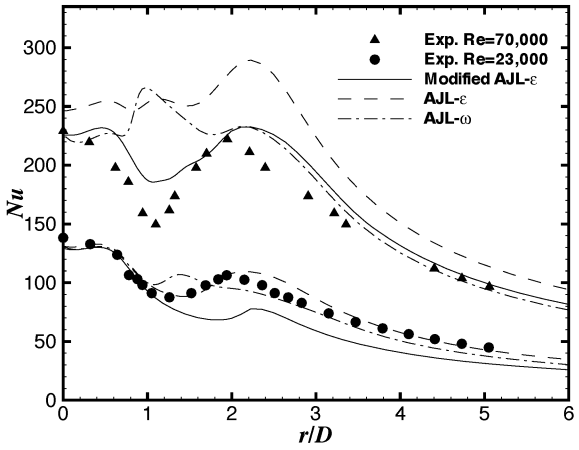

Figure 9: Nusselt number profile in the impinging jet at $Re = 23,000$ and $Re = 70,000$ $(H/D = 2.0)$

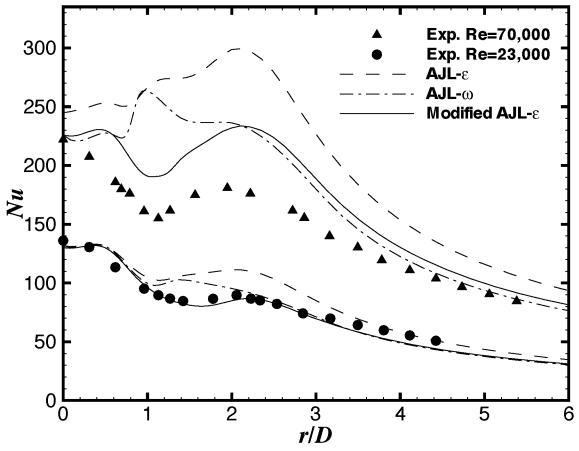

Figure 10: Nusselt number profile in the impinging jet at $Re = 23,000$ and $Re = 70,000$ $(H/D = 4.0)$

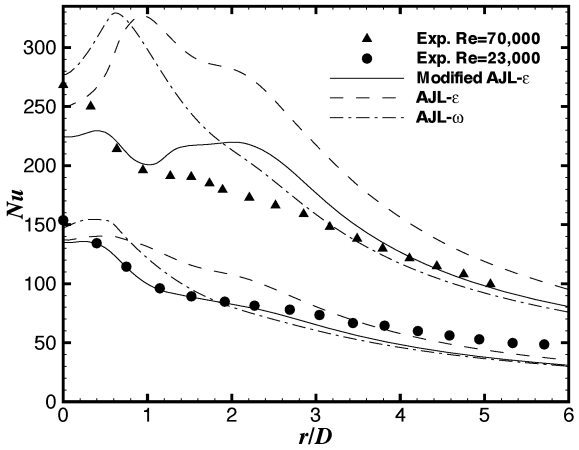

Figure 11: Nusselt number profile in the impinging jet at $Re = 23,000$ and $Re = 70,000$ $(H/D = 6.0)$

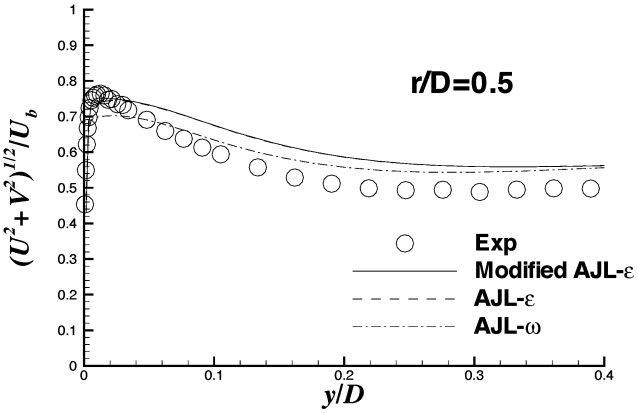

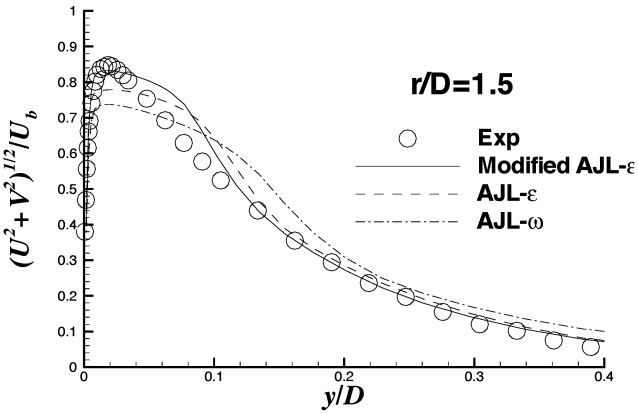

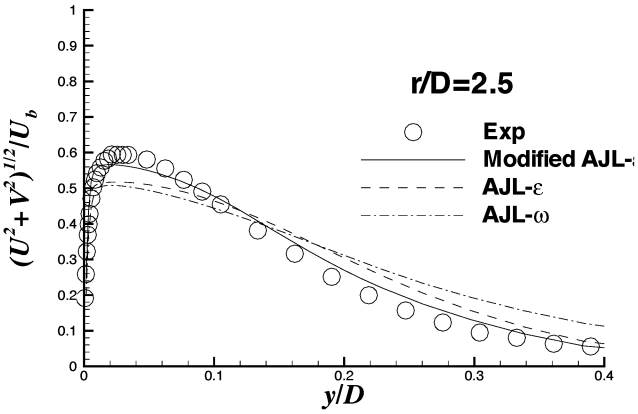

Figure 12: Mean velocities in the impinging jet $H/D = 6$ $(Re = 70,000)$